Materials Science-Poland, Vol. 23, No. 4, 2005

Synthesis and ESR study of $(Tb_xY_{1-x})_2Cu_2O_5$ solid solutions

J. TYPEK[1*], J. KOSTRZEWA[1], N. GUSKOS[1, 2]

[1]Institute of Physics, Szczecin University of Technology, al. Piastów 17, 70-310 Szczecin, Poland

[2]Solid State Section, Department of Physics, University of Athens, Panepistimiopolis, 15 784 Zografos, Athens, Greece

Polycrystalline samples of $(Tb_xY_{1-x})_2Cu_2O_5$, where x = 1.0, 0.75, 0.50, 0.38, 0.25, 0.125 and 0, were synthesized by the solid-state reaction technique. XRD measurements showed that the obtained samples are single-phase and belong to the orthorhombic space group *Pna*2_1. The observed linear change of the lattice parameters and unit cell volume with terbium concentration is in agreement with Vegard's law. A thermogravimetric study of the decomposition process of the obtained samples revealed small sample-dependent mass losses in the temperature range 1030–1050 °C, and a larger, intrinsic mass loss in the range 1100–1150 °C. The former are probably due to the $4\ CuO \longrightarrow 2\ Cu_2O + O_2$ transformation, while the latter is related to the reaction $2Y_2Cu_2O_5 \longrightarrow 4YCuO_2 + O_2$. The peak temperature of the main decomposition stage varies linearly with terbium concentration, which could be explained by an increasing distortion of coordination polyhedra around the copper ion, caused by the substitution of the larger Tb^{3+} cation. The ESR spectra of $(Tb_xY_{1-x})_2Cu_2O_5$ solid solutions showed a complicated structure due to the presence of various copper clusters (tetramers, trimers). Moreover, the ESR spectra were anisotropic in an external magnetic field, despite originating from powder samples.

Key words: *solid solutions; ESR; copper complexes*

1. Introduction

The discovery of high-temperature superconductivity in $RBa_2Cu_3O_7$ compounds (where R is a rare earth element) has greatly increased interest in other non-superconducting copper oxides. $R_2Cu_2O_5$ compounds with the orthorhombic space group *Pna*2_1 include a well known "blue phase", $Y_2Cu_2O_5$, often found as a common second phase in the synthesis of $YBa_2Cu_3O_7$. The family of the orthorhombic $R_2Cu_2O_5$ compounds includes those with rare-earth R^{3+} cations smaller then Gd, i.e. Tb, Dy, Ho, Y,

[*]Corresponding author, e-mail: typjan@ps.pl.

Er, Tm, Yb, as well as with Lu, In, and Sc [1–3]. The most characteristic feature of the $R_2Cu_2O_5$ crystallographic structure is the occurrence of zigzag copper chains along the *a*-axis (Fig. 1). There is a distorted square planar arrangement of four oxygen atoms around copper atoms, with the fifth oxygen atom forming a sort of a pyramid. These copper–oxygen pyramids are joined at their common edges into Cu_2O_8 dimers. The dimers, through the bridging oxygen, form an infinite zigzag Cu_2O_5 copper –oxygen chains. Furthermore, each copper atom is coupled with four other Cu ions along the *b*-axis, forming *ab*-pseudoplanes. The rare earth ions are octahedrally coordinated, and these distorted RO_6 octahedra are linked in a three-dimensional network occupying the space between copper–oxygen planes [3].

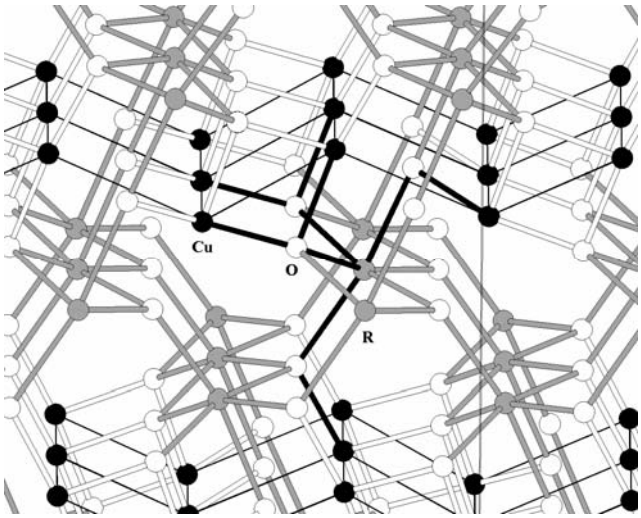

Fig. 1. The crystal structure of $R_2Cu_2O_5$ compounds

All $R_2Cu_2O_5$ compounds are antiferromagnetically ordered at low temperatures and most of them exhibit metamagnetic behaviour below the Neel temperature [4]. The magnetic properties of $Y_2Cu_2O_5$ have been studied extensively [4–10]. Above 120 K, the magnetic susceptibility of this compound is well described by the Curie–Weiss law with a positive Curie temperature, θ = 38.5 K, indicating a considerable contribution of ferromagnetic interaction [4]. At T_N = 11.5 K a sharp maximum in the susceptibility gives a strong indication of an antiferromagnetic ordering. In the antiferromagnetic state two jumps in the $M(H)$ magnetization curve (with the external field H applied along *b*-axis) are observed, corresponding to the two metamagnetic transitions [10]. The magnetic studies of $Tb_2Cu_2O_5$ have been presented in Refs. [11–17]. The magnetic susceptibility of this compound containing two magnetic ions follows the Curie–Weiss law with the antiferromagnetic transition temperature T_N = –10 K. Transition to the antiferromagnetic phase was reported to take place in the 17–21.5 K temperature range. An additional anomaly of magnetic susceptibility was observed in the 5–8 K range. The magnetic structure in an ordered state of $R_2Cu_2O_5$ compound could be viewed as consisting of ferromagnetic CuO layers

parallel to the *ab*-plane coupled antiferromagnetically. The copper magnetic moments are aligned along the *b*-axis (at least for R = Y, Lu, Er, Tb). Despite a large amount of experimental material gathered from magnetic susceptibility and neutron diffraction measurements, the understanding of the nature of magnetic interactions in the $R_2Cu_2O_5$ family is still incomplete.

Conventional X-band electron spin resonance (ESR) has been used to study the magnetic properties of $Y_2Cu_2O_5$ in the paramagnetic state, the sample being in the form of powder [15–22] or single crystals [23, 24]. For the investigation of the antiferromagnetic state, antiferromagnetic resonance (AFMR) was employed [23–26]. At room temperature, a single Lorentzian-shape ESR line, centred at g = 2.13, with a linewidth of ΔB = 90 mT, was recorded. As the temperature was decreased to 50 K, the *g*-value and the linewidth remained virtually unchanged. Below 40 K, the line started to broaden and the *g*-value shifted to 2.0 [19]. For certain samples, a number of weaker lines, supposedly arising from clusters of four copper ions coupled by a superexchange interaction through interviewing oxygen ions (copper tetramers), have been detected [21, 22]. Such clusters could form in those portions of the sample in which the oxygen content is reduced. AFMR modes have been analysed in a model assuming the existence of S = l dimers formed by two Cu^{2+} spins. In the Cu^{2+} chains along the *a*-axis, due to 90° and 180° Cu–O–Cu exchange paths, there are alternative strong ferromagnetic (J_0 = 340 K) and weak antiferromagnetic (J_1 = –0.33 K) interactions. Such a model of spin system is capable of showing metamagnetic transitions, although discrepancies between the experimental and calculated results exist [23, 25].

Compositional series of solid solutions of $(R_xR'_{1-x})_2Cu_2O_5$ -type, where R and R' are different rare earth ions, have been the subject study of only a few papers [27-29]. The structure and magnetic properties of $(In_xY_{1-x})_2Cu_2O_5$ compounds were reported in the temperature range between 77 K and room temperature [27]. In another work it was found that the maximum solubility of Gd in $Y_2Cu_2O_5$ is $x \approx 0.3$ and that the low -temperature magnetic phase diagram of $(Gd_xY_{1-x})_2Cu_2O_5$ was established [28]. Within samples of $(Ca_xY_{1-x})_2Cu_2O_5$, where x = 0.05, 0.1 and 0.2, a phase with incommensurate modulated structure has been found [29]. This phase becomes the main phase within the $(Ca_{0.2}Y_{0.8})_2Cu_2O_5$ sample. In the present paper, an attempt has been taken to synthesize $(Tb_xY_{1-x})_2Cu_2O_5$ for the whole range of the terbium index x. Combining a magnetic Tb ion and a non-magnetic Y ions could be especially interesting, because they would allow to investigate the magnetic interaction between the d (Cu) and f (Tb) ions present in the solid solutions. We present X-ray, thermogravimetric, and ESR measurements of the obtained samples and discuss their results.

2. Experimental

Ceramic samples of $(Tb_xY_{1-x})_2Cu_2O_5$ have been prepared by heating in air appropriate stoichiometric amounts of Y_2O_3 (99.99%), Tb_2O_3 (99.99%), and CuO (99.99%) at 1000 °C. The samples with the following values of the terbium index x have been

prepared: x = 1.0, 0.750, 0.50, 0.38, 0.25, 0.125 and 0. Four intermediate grindings and pressings were carried out to homogenize the reaction products. The total firing time was about 100 hours in order to get a complete reaction of the starting powders. The heating was carried out in a Carbolite CTF 12/100/900 tube furnace. An Eurotherm 902P temperature controlled the temperature programs.

X-ray studies were carried out on a Dron-3 diffractometer using $Co_{K\alpha}$/Fe radiation at room temperature. The X-ray patterns were taken by means of step-scanning the sample using the θ–2θ method with a step of 0.02°.

The thermal analysis (simultaneous TGA-DSC measurements) was conducted on a Setaram apparatus model TG 92-16. All measurements were recorded at 4 °C/min under dry synthetic air (N_2:O_2 = 80:20 % vol.) or argon flow in 20–1200 °C temperature range. The ceramic samples (m = 50.7±0.1 mg) were held in a platinum cylinder and placed in 17 cm^3/min gas flow stream. Kinetic parameters of sample decomposition were calculated using a computer program Setsoft Kinetics on DTG by Setaram.

The ESR room temperature experiments were performed on a Bruker E 500 spectrometer operating at X-band microwave frequency equipped with TE_{102} cavity with 100 kHz field modulation. Each sample was in form of loose powder and during the measurements they were placed in quartz tubes.

3. Results and discussion

Solid solutions $(Tb_xY_{1-x})_2Cu_2O_5$ could be synthesized for the whole range of Tb concentration, $0 < x < 1$, showing in all cases a single phase. The X-ray patterns were indexed in the orthorhombic symmetry. Figure 2 presents, as an example, the obtained

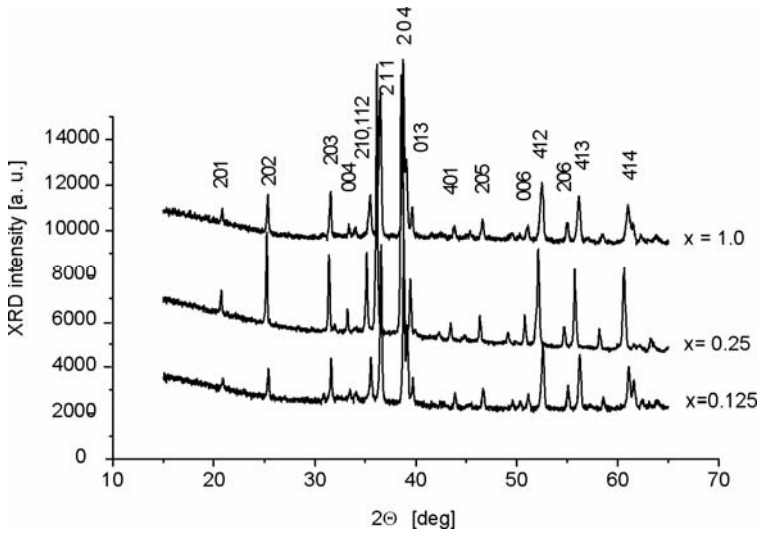

Fig. 2. XRD patterns for the three investigated samples of $(Tb_xY_{1-x})_2Cu_2O_5$. Peaks labelled by the indices *hkl* were used for calculating the lattice parameters

XRD spectra for three selected samples of $(Tb_xY_{1-x})_2Cu_2O_5$. Lattice spacing d_{hkl} was calculated by the Bragg law using all of the 16 peaks labelled in Figure 2. The lattice parameters of the unit cell, *a*, *b* and *c*, were determined by simultaneously fitting the lattice spacing to the following expression for an orthorhombic crystal,

$$\frac{1}{d_{hkl}} = \frac{h^2}{a^2} + \frac{k^2}{b^2} + \frac{l^2}{c^2}$$

with a non-linear least-square fitting procedure.

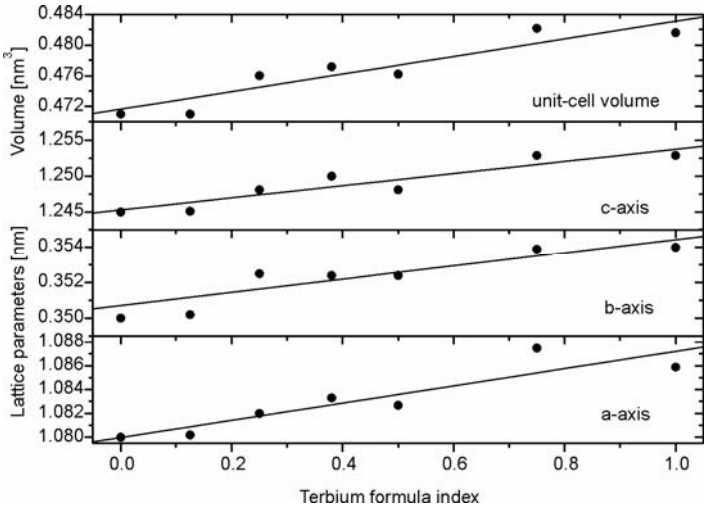

Fig. 3. The variation of the unit cell volume (top panel) and lattice parameters (lower panels) with the terbium index *x*

Figure 3 presents the change of the unit cell volume (top panel) and the unit cell parameters (lower three panels) with the terbium index. The linear increase of these parameters with increasing terbium concentration is in agreement with the larger Tb^{3+} ionic radius (0.923 Å in six-fold coordination) compared to Y^{3+} (0.90 Å). The values of the cell parameters obtained for the limiting ranges of $x = 0$ and $x = 1$ terbium indexes agree with the previous structural data on the $Tb_2Cu_2O_5$ and $Y_2Cu_2O_5$ compounds [3]. The linear change of the lattice parameters and the unit cell volume with the *x* index is in agreement with Vegard's law.

Figure 4 presents the differential thermogravimetry (DTG) curves taken during the heating run for five samples in the 1000–1200 °C range. The observed decomposition of the samples is connected with the endothermic processes and could be divided into three stages. The first two stages, which are sample-dependent, are connected with a small mass loss occurring in the 1030–1050 °C temperature range. The third, main stage of the decomposition is intrinsic. It is related to a larger mass loss that takes place at higher temperatures, above 1100 °C.

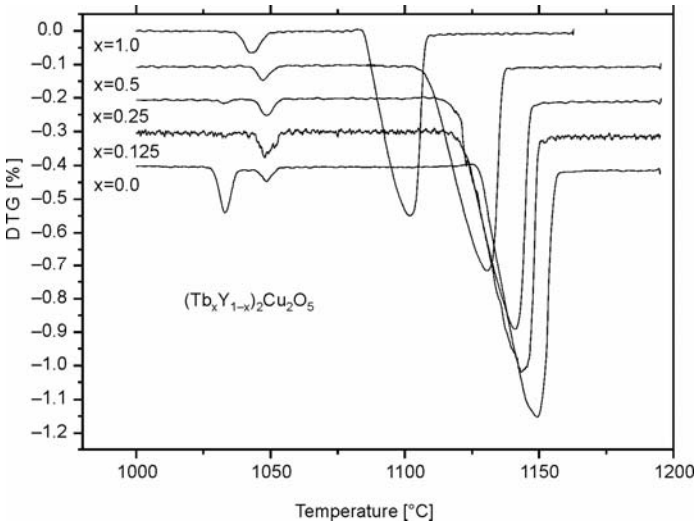

Fig. 4. The DTG traces of $(Tb_xY_{1-x})_2Cu_2O_5$ for five various terbium concentrations. The recordings for $x \neq 1.0$ have been vertically shifted for better visibility

To analyse the obtained DTG curves the Freeman–Carroll method was used, which enables calculation of the reaction order and the activation energy of a decomposing material. The method is based on the following equation for the mass losses:

$$\frac{dm}{dt} = k_0 c^n \exp\left(\frac{E_a}{RT}\right)$$

where n is the reaction order, E_a is the activation energy, and the other symbols have their usual meanings. The calculated values of the main parameters of this equation for the observed three decomposition stages are presented in Table 1. The temperature of the top of the respective DTG peak is designated as T_p. It was found that for the main decomposition stage this temperature varies linearly with the terbium index x (Fig. 5). The obtained values of activation energy for the first two decomposition stages are unrealistically high. As these stages are sample-dependent and a complete chemical and physical characterization of specific samples is lacking, these values must be treated as apparent, not corresponding to real, physically identifiable processes.

Table 1. DTG data for the decomposition processes of the investigated samples

Parameter	I stage	II stage	III stage
Stage character	sample-dependent	sample-dependent	intrinsic
Relative mass loss [%]	0.0–0.18	0.0–0.25	1.90–3.20
T_P [K]	1030–l035	1043–1049	1100–1150
E_a [kJ/mol]	6300–7800	6000–8100	1520–2180
n	1.60–1.90	1.40–1.90	0.40–0.70

The Y–Cu–O ternary can be effectively represented as Y_2O_3 –Cu–O–Cu ternary subsystem below 1 bar oxygen pressure. In this subsystem there are six phases: Y_2O_3, CuO, and $Y_2Cu_2O_5$, which are stable in the air, and Cu metal, Cu_2O and $YCuO_2$, which is only stable at lower oxygen pressure [30]. Oxygen coulometric investigations showed that the $YCuO_2$ is the problem phase, which is easily retained, or even formed under metastable conditions. This metastable $YCuO_2$ disturbs the low-temperature equilibrium of the $Y_2Cu_2O_5$ phase, thus leading to large uncertainty observed for the decomposition temperature of $Y_2Cu_2O_5$ [30]. Lysenko has presented the phase diagram of CuO–$YO_{1.5}$ system at 21 kPa oxygen pressure [31]. For CuO-rich compounds a phase line separates CuO + $Y_2Cu_2O_5$ and Cu_2O + $Y_2Cu_2O_5$ phases at 1027°C. Around 1130°C the decomposition of $Y_2Cu_2O_5$ into $YCuO_2$ occurs. Based on this phase diagram, one of the sample-dependent stages of decomposition recorded for $(Tb_xY_{1-x})_2Cu_2O_5$ could be explained as a result of transformation of excess CuO into Cu_2O, according to the reaction $4CuO \rightarrow 2Cu_2O + O_2$. In samples, where no excess of CuO is present that decomposition stage is missing.

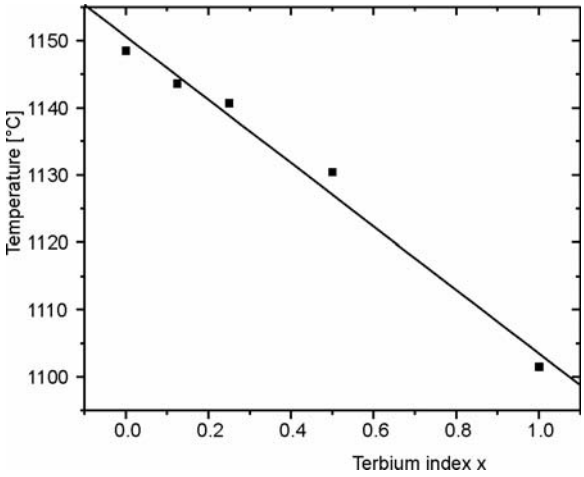

Fig. 5. The dependence of the temperature T_p of the main decomposition DTG peak (third stage) on the terbium index x

On the other hand, the main decomposition stage intrinsic to all samples is probably related to the transformation of $Y_2Cu_2O_5$ into $YCuO_2$, according to the reaction $2Y_2Cu_2O_5 \rightarrow 4YCuO_2 + O_2$. During this stage the oxygen atoms from the bulk of the sample are released causing an irreversible change in the crystal structure. This is confirmed by a quite different X-ray diffractogram of the sample heated above 1200 °C in comparison with the starting diffractogram. Also the ESR spectrum of the overheated sample vanishes after that treatment.

Lowering of the decomposition temperature with the increasing concentration of terbium (Fig. 5) could be most simply seen as a result of lower stability caused by an increased distortion around copper ions. There is a large distortion of coordination

polyhedra around Cu^{2+} in $R_2Cu_2O_5$ compared to that in tenorite (CuO). This distortion increases as the ionic radius of the R^{3+} cation increases. This means that the enthalpy of formation of $Y_2Cu_2O_5$ from the component oxides must increase as the ion radius of R^{3+} increases [32]. This agrees with the results obtained from the structural parameters [3]. Thus substitution of larger ion (Tb^{3+}) for a smaller ion (Y^{3+}) makes the structure less stable and lowers the decomposition temperature.

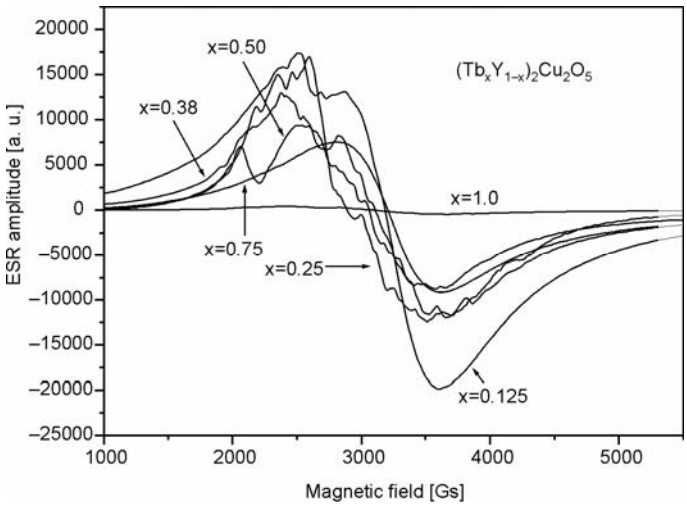

Fig. 6. The ESR spectra for $(Tb_xY_{1-x})_2Cu_2O_5$ solid solutions for various terbium indices x

The ESR spectra of $(Tb_xY_{1-x})_2Cu_2O_5$ solid solutions for various terbium concentrations are presented in Figure 6. Although the spectra are fairly complicated, the overall tendency of decreasing the ESR intensity with increasing terbium concentration is easily to notice. For $x = 1$ the sample is ESR silent. Similar tendency was observed previously for the $(Er_xY_{1-x})_2Cu_2O_5$ and $(Dy_xY_{1-x})_2Cu_2O_5$ compounds [33, 34]. It was found that the relative ESR signal intensity $I(x)$ varies with the magnetic rare earth ion concentration index x according to a simple power law function, $I(x) \sim (1 - x^{1/n})$, where n is the number of the superexchange paths between R^{3+} and Cu^{2+} ions [34]. In the case of the $(Tb_xY_{1-x})_2Cu_2O_5$ compound this dependence does not apply because a large part of the ESR signal arises from the copper defect clusters, among them copper tetramers [22]. Copper tetramers, consisting of copper ions coupled by intervening oxygen ions by an exchange interaction, were identified in $Y_2Cu_2O_5$ powder through sets of four ESR resonance lines. They were interpreted as the fine structure of $S = 2$ system [22]. It was noticed that the emergence of these signals depends upon the oxygen content of the sample, particularly when it is reduced.

The investigated samples of $(Tb_xY_{1-x})_2Cu_2O_5$, although in a ceramic form, showed a significant angular dependence in an external magnetic field. Figure 7 presents the angular anisotropy for the $TbYCu_2O_5$ compound. Successive rotations of the sample

by 30° along the axis perpendicular to the steady magnetic field produces significant changes in the ESR spectrum. Such behaviour is known for other powder or ceramic systems and is explained by the texturing of disk-like particles during the technological operations of pressing and sintering [35]. Since the observed spectra are not fully resolved and there is a superposition of different components, the analysis of the ESR signals could not be very detailed. Considering the overall spread of component lines in the magnetic field, it could be estimated that the value of the zero-field splitting parameter D for tetramers is smaller than 0.05 cm^{-1}. A complex spectrum of the $TbYCu_2O_5$ sample also indicates the presence of trimer copper clusters ($S = 3/2$), evidenced by the appearance of sets of three lines. For such a cluster, the value of D must be smaller than 0.006 cm^{-1}.

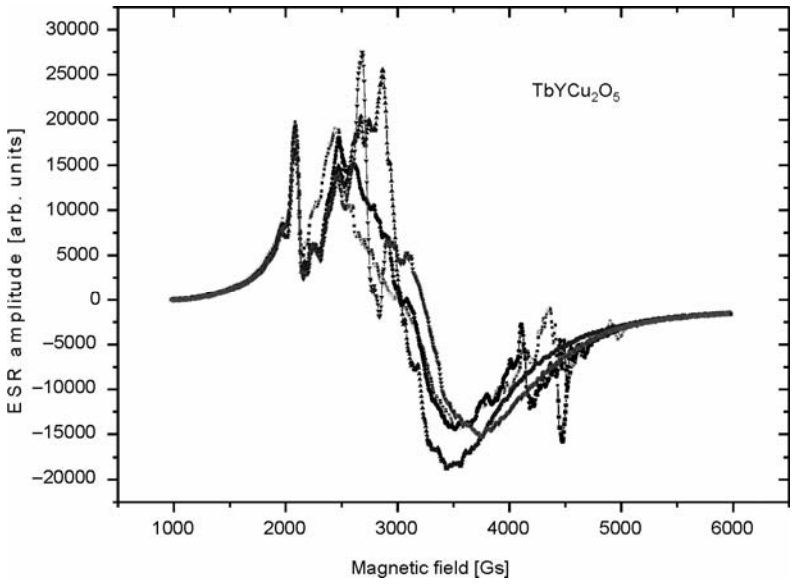

Fig. 7. The angular anisotropy of the ESR spectrum for the $TbYCu_2O_5$ compound. The sample has been successively rotated by 30° along the axis perpendicular to the steady magnetic field between each recording

In conclusion, the synthesis and characterization of $(Tb_xY_{1-x})_2Cu_2O_5$ copper oxides in the whole compositional range of terbium concentration, $1 \geq x \geq 0$, has been performed. The compounds were characterized by XRD, thermogravimetric, and ESR measurements, verifying the existence of a solid solution series, while room temperature ESR data suggest the presence of magnetic defects in the form of copper clusters.

References

[1] BERGERHOFF G., KASPER H., Acta Crystallogr., B 24 (1968), 388.
[2] FREUD H.R., MULLER-BUSCHBAUM H., Z. Naturforsch., B 32 (1977), 609.

[3] GARCIA-MUNOZ J.L., RODRIQUEZ-CARVAJAL J., J. Solid State Chem., 86 (1990), 310.
[4] TROC R., KLAMUT J., BUKOWSKI Z., HORYN R, STEPIEN-DAMM J., Physica, B 154 (1989), 189.
[5] KAZEI Z.A., KOLMAKOVA N.P., LEVITAN R.Z., MILL B.V., MOSHCHALKOV V.V., ORLOV V.N., SNEGIREV V.V., ZOUBKOVA JA., J. Magn. Magn. Mater., 86 (1990), 124.
[6] GARCIA-MUNOZ J.L., RODRIGUEZ-CARVAJAL J., OBRADORS X., Phys. Lett., A 149 (1990), 319.
[7] HORYN R., KLAMUT J., WOLCYRZ M., WOJAKOWSKI A., ZALESKI A.J., Physica, B 205 (1995), 51.
[8] BARAN M., LEVITIN R.Z., MILL B.V., SZYMCZAK R., Zh. Eksp. Teor. Fiz., 109 (1996), 961.
[9] SZYMCZAK R., SZYMCZAK H., BARAN M., LEVITIN R.Z., MILL B.V., J. Magn. Magn. Mater., 157–158 (1996), 667.
[10] MATSUOKA Y., NISHIMURA Y., MITSUDO S, NOJIRI H., KOMATSU H., MOTOKAWA M., KAKURAI K., NAKAJIMA K., KARASAWA Y., NIIMURA N., J. Magn. Magn. Mater., 177–181 (1998), 729.
[11] MOSHCHALKOV V.V., SAMARIN N.A., GRISHCHENKO I.O., J. Magn. Magn. Mater., 90–91 (1990), 533.
[12] GOLOSOVSKII I.V., MILL B.W., PLAKHTII W.P., KHARCHENKOV W.P., Fiz. Tver. Tela, 33 (1991), 3412.
[13] CHEPURKO G.G., PAUKOV I.U., POPOVA M.N., ZOUBKOVA JA., Solid State Commun., 79 (1991), 569.
[14] ZOUBKOVA JA., KRINETSKII I.B., LEVITIN R.Z., Fiz. Tver. Tela, 34 (1992), 1361.
[15] BOWDEN G.J., ELLISTON P.R., WEN K.T., DOU S.X., ESTERLINK K.E., BOURDILLON A., SORRELL C.C., CORNELL B.A., SEPAROVIC F., J. Phys. C: Solid State Phys., 20 (1987), L545.
[16] RAMAKRISHNA B.L., ONG E.W., Solid State Commun., 68 (1988), 775.
[17] ARIDE J., FLANDROIS S., TAIBI M., BOUKHARI A., DRILLON M., SOUBEYROUX L.J., Solid State Commun., 72 (1989), 459.
[18] GENOSSAR J., SHALTIEL D., ZEVIN V., GRAYEVKY A., FISHER B., J. Phys.: Condens. Matter, 1 (1989), 9471.
[19] GANGULY P., SREEDHAR K., RAJU A., DEMAZEAU G., HAGENMULLER P., J. Phys.: Condens. Matter, 1 (1989), 213.
[20] HOFFMANN S.K., CZYZAK B., STANKOWSKI J., Acta Phys. Polon., A 77 (1990), 621.
[21] SINGH R.J., IKRAM M., PUNNOOSE A., MAURYA B.P., KHAN S., Phys. Lett., A 208 (1995), 369.
[22] IKRAM M., SINGH R.J., Indian J. Pure Appl. Phys., 37 (1999), 622.
[23] KIMURA S., OHTA H., MITSUDO S., MOTOKAWA M., JANG W-J., HASEGAWA M., TAKAEI H., J. Phys.: Condens. Matter, 8 (1996), 5461.
[24] KIMURA S., OHTA H., MOTOKAWA M., MITSUDO S., JANG W.J., HASEGAWA M., TAKEI H., Int. J. Infrared Millimeter Spectr., 17 (1996), 833.
[25] KIMURA S., KANEKO K., OHTA H., MOTOKAWA M., Physica, B 201 (1994), 115.
[26] KIMURA S., OHTA H., MOTOKAWA M., J. Phys. Soc. Japan, 65 (1996), 297.
[27] SU Q., CAO X., WANG H., J. Solid State Chem., 111 (1994), 310.
[28] HORYN R., KLAMUT J., WOLCYRZ M., WOJAKOWSKI A., ZALEWSKI A.J., J. Magn. Magn. Mater., 140–144 (1995), 1575.
[29] FENG C.N., LOVETT D.R., Phys. Stat. Sol., (a) 167 (1998), 3.
[30] KONETZKI R.A., SCHMIDT-FETZER R., J. Solid State Chem., 114 (1995), 420.
[31] LYSENKO W.A., Inorg. Mat., 35 (1999), 1076.
[32] KALE G.M., J. Solid State Chem., 125 (1996), 13.
[33] TYPEK J., BUCHOWSKI D., GUSKOS N., SZYMCZYK A., WABIA M., Radiation Eff. Defects Sol., 158 (2003), 105
[34] TYPEK J, KOSTRZEWA J, SZYMCZYK A., GUSKOS N., Mol. Phys. Rep., 39 (2004), 233
[35] KAKAZEY M., VLASOVA M., GONZALEZ-RODRIGUEZ G., SALAZAR-HERNANDEZ B., Mat. Sci. Eng., B 90 (2002), 114

Received 23 September 2004
Revised 25 January 2005